Hindawi Publishing Corporation
International Journal of Antennas and Propagation
Volume 2014, Article ID 301934, 10 pages
http://dx.doi.org/10.1155/2014/301934

*Research Article*

# Application of Hybrid Finite Element-Boundary Integral Algorithm for Solving Electromagnetic Scattering from Multiple Objects over Rough Sea Surface

**Run-Wen Xu and Li-Xin Guo**

*School of Physics and Optoelectronic Engineering, Xidian University, Xi'an 710071, China*

Correspondence should be addressed to Run-Wen Xu; rwxu719@126.com

Received 23 April 2014; Revised 9 July 2014; Accepted 25 July 2014; Published 13 August 2014

Academic Editor: Timothy Field



A hybrid algorithm of the finite element method (FEM) is presented to solve two-dimensional (2D) scattering from multiple dielectric objects above the rough sea surface. Compared with traditional FEM based on approximate absorbing boundaries, FEM based on the boundary integral method (BIM) can reduce the calculational region and solution time of the scattering problem. In the hybrid method, the whole computational region is divided into the sea surface and multiple isolate interior regions for the dielectric objects. FEM is only used to simulate the scattering from multiple interior regions enclosing the objects, whereas the large sea is considered exactly by BIM. The coupled interaction among the isolate interior regions and the sea can be taken into account by BIM. The hybrid technique presented here is efficient and versatile for addressing scattering from multiple arbitrary targets above rough sea surfaces. Scattering properties of multiple dielectric objects above the sea surface under different conditions are discussed in detail.

## 1. Introduction

Modeling of the electromagnetic scattering and radiation from objects above the rough surface is very important in many signal processing applications, such as target detection and tracking, imaging and remote sensing, and electronic countermeasures. Several numerical methods, such as the method of moments (MoM) [1], the method of multiple interactions (MOMI) [2], the fast multiple method (FMM) [3], and the forward-backward method (FBM) [4], have been published in some literatures to study electromagnetic scattering from rough surfaces or an object above a rough surface. Although these methods based on the boundary integral method (BIM) can be applied easily and exactly to analyze the scattering from a perfectly electric conducting (PEC) model, they are difficult to simulate the dielectric models, and their general applications are not very ideal. Many valuable papers [1–4] about the scattering properties of the rough surfaces have been published, but little information is provided for the scattering problems of dielectric objects above the sea surfaces based on boundary integral methods.

The finite element method (FEM) can easily be used for analyzing complex dielectric problems because of its powerful ability to model inhomogeneous materials that may be difficult to solve by the classical BIM. In traditional applications of FEM, approximate absorbing boundaries, such as ABC [5, 6] and PML [7–10], were usually adopted to truncate the infinite domain when electromagnetic scattering problems were discussed with FEM. FEM/PML was used to simulate the bistatic scattering from a PEC object above the rough sea surface [7]. The scattering from objects on/above rough sea surfaces was analyzed by the Monte Carlo-based characteristic basis FEM in [10]. To maintain their precisions, approximate absorbing boundaries must often be set sufficiently far from the model surface. However, these boundaries suffer from a large number of unknowns and require vast computational memory, especially for the scattering problem of a large model. The finite element

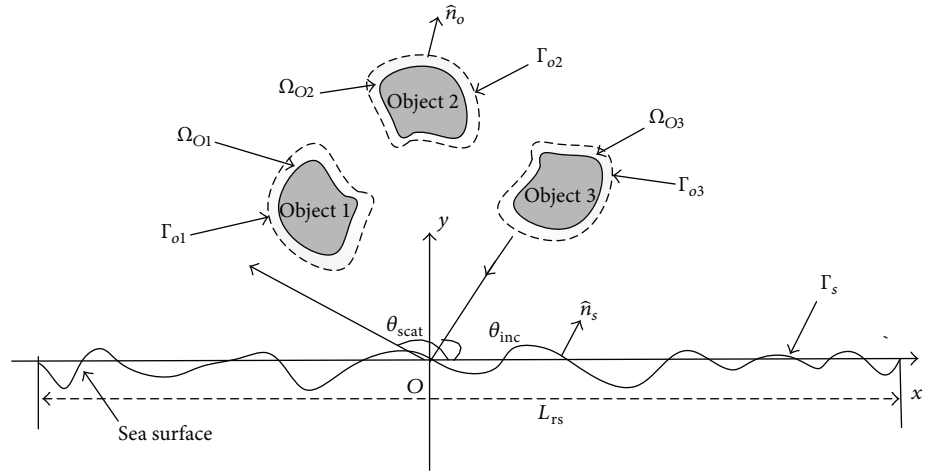


Figure 1: Geometry of scattering from multiple objects above rough sea surface.

method combined with the boundary integral method (FEM/BIM) has recently been paid increased attention to its application in electromagnetic scattering problems. As the most accurate boundary, the application of the truncated boundary obtained by BIM in FEM can not only deal with the complex model easier than BIM but also maintain high precision and be set near the model surface to reduce the computation region. A symmetric FEM/BIM formulation [11] was presented to solve the scattering from objects and accelerated using a single level QR algorithm. A preconditioned formulation of FEM/BIM with the nonoverlapping and nonconforming domain decomposition method (DDM) [12] was proposed to calculate the electromagnetic scattering from cavities. A flexible and efficient higher order FEM/BIM with multilevel fast multipole algorithm [13] was applied to solve the scattering problem of a large body with deep cavities. In previously published studies, only objects or plane surfaces were discussed by FEM/BIM, and few papers have discussed the scattering problem of multiple targets over rough surfaces. Numerical simulations for the composite scattering based on this hybrid method require further study. Some work has been done for the scattering from the rough surface by our team. In [14], an initial study of the application of FEM/BIM was presented which was only focused on the scattering from the rough surface. The modeling method in [14] applied an artificial boundary to enclose the whole model, which can be hardly used in the composite model of multiple objects above the rough surface because it consumes lots of computer memory and time. The composite scattering from an arbitrary dielectric target above the rough surface was analyzed by FEM/PML in [15], and it applied a comparison of the hybrid method in this paper. In [16], we used the FEM/BIM to study the scattering from objects buried under a Gauss rough ground which can provide a good way for this paper. Study on electromagnetic scattering from objects above the rough surface becomes more and more important in many applications. In this paper, the model of multiple objects above the Pierson-Moskowitz (PM) rough sea surface is generated, and the scattering properties of the compositing model are analyzed in detail.

In this paper, hybrid FEM/BIM is introduced to simulate the scattering from multiple objects above the sea surface based on previous studies [11–16]. In the hybrid method, the computational domain is divided into the sea surface and many isolated computational subspaces containing the objects. For isolated regions surrounded by fictitious boundaries, FEM is used to solve the problem, while BIM is used to analyze the scattering from the sea. The fields among these isolated enclosed regions are strongly or weakly coupled by the integral boundaries. Compared with traditional FEM, only the isolated regions containing the objects need to be analyzed by FEM, which can reduce both memory and computational time. The strategy of hybrid FEM/BIM and the modeling method are presented with the validity of our codes evaluated by FEM/PML. The scattering properties of multiple dielectric objects over the sea are then investigated.

## 2. Scattering of Multiple Targets above the Rough Sea Surface

In the traditional finite element approach, artificial boundaries usually enclose the entire region of the objects and the underlying rough surface. The enclosed computed region is quickly increased when the object is far from the underlying rough surface, especially when multiple objects exist. To avoid this situation, the computational domain is divided into many isolated subspaces as shown in Figure 1 which depicts a general two-dimensional (2D) scattering schematic of multiple dielectric objects with arbitrary shapes over the rough sea surface.

The incident wave impinges upon the composite model with an incidence angle $\theta_{\text{inc}}$ and scatted by a scattering angle $\theta_{\text{scat}}$. The symbols $\hat{n}_o$ and $\hat{n}_s$ represent the unit normal vectors. The interior region $\Omega_{o_i}$ is defined as the region of the $i$th object. $\Gamma_s$ denotes the truncated part of the sea. The fictitious boundary $\Gamma_{o_i}$ is the artificial boundary enclosing the $i$th object. As the most precise truncated boundaries, the integral boundaries can be arranged at a very close distance from the model surface and set evenly on the object surface. Doing so

has little effect on the precision of the results, so fictitious boundaries $\Gamma_{o_i}$ are set on the surface of each object in our simulation to minimize the computational region as much as possible.

In our model, the PM rough sea surface can be generated based on the Monte Carlo technique [17]. The sea surface is truncated into a finite computational domain when the FEM is applied which can introduce artificial reflection. To reduce the truncation effect, we use a tapered incident wave [18] as the incident wave which is expressed as

$$\Phi^{\text{inc}} = \exp\left[i\mathbf{k}\cdot\mathbf{r}\left(1+w\left(\mathbf{r}\right)\right)\right]\cdot\exp\left[-\frac{\left(x-yctg\theta_{\text{inc}}\right)^2}{g^2}\right], \tag{1}$$

where $w(\mathbf{r}) = [2(x - yctg\theta_{\text{inc}})^2/g^2 - 1]/(kg\sin\theta_{\text{inc}})^2$, $g$ is the tapered factor, and $\mathbf{r}$ is the position vector. Another advantage of adopting the tapered incident wave is that the parts of the sea overflowing from the truncated region can be eliminated because the amplitude of the incident wave on these parts decreases to a very small value.

Considering that the electric field has a single component along the axis of $z$, the electric field integral equation (EFIE) [17] for the multiobject scattering problem can be obtained by

$$\begin{aligned}\Phi_{\Gamma_o+\Gamma_s}\left(\mathbf{r}'\right) = &-\int_{\Gamma_s} G_0\left(\mathbf{r},\mathbf{r}'\right)\frac{\partial}{\partial n}\Phi\left(\mathbf{r}\right)d\Gamma \\ &+\sum_{i=1}^{m}\int_{\Gamma_{o_i}}\left[\Phi\left(\mathbf{r}\right)\frac{\partial G_0\left(\mathbf{r},\mathbf{r}'\right)}{\partial n}\right. \\ &\left.-G_0\left(\mathbf{r},\mathbf{r}'\right)\frac{\partial}{\partial n}\Phi\left(\mathbf{r}\right)\right]d\Gamma \\ &+\Phi^{\text{inc}}\left(\mathbf{r}'\right),\end{aligned} \tag{2}$$

where $\Phi^{\text{inc}}(\mathbf{r}') = -\iint_{\Omega}[G_0(\mathbf{r},\mathbf{r}')f(\mathbf{r})]d\Omega$, and $m$ denotes the total number of objects. The given integral equation provides a relationship between the electromagnetic field on the artificial boundary and its normal derivative. The coupled interaction of fields among subdomains can be taken into account in (2).

In our discussion, the truncated boundary condition on the artificial surface $\Gamma$ can be assumed as follows for simplification:

$$\left.\frac{\partial\Phi}{\partial n}\right|_{\Gamma} = -\psi. \tag{3}$$

Substituting (3) into (2), the integral equation can be written as

$$\begin{aligned}\Phi_{\Gamma_o}\left(\mathbf{r}'\right) = &\int_{\Gamma_s} G_0\left(\mathbf{r},\mathbf{r}'\right)\psi\left(\mathbf{r}\right)d\Gamma \\ &+\sum_{i=1}^{m}\int_{\Gamma_{o_i}}\left[\Phi\left(\mathbf{r}\right)\frac{\partial G_0\left(\mathbf{r},\mathbf{r}'\right)}{\partial n}+G_0\left(\mathbf{r},\mathbf{r}'\right)\psi\left(\mathbf{r}\right)\right]d\Gamma \\ &+\Phi^{\text{inc}}\left(\mathbf{r}'\right).\end{aligned} \tag{4}$$

Therefore, the above equation can be discretized using the basis functions as in [19], and (4) can be represented in matrix notation as

$$\left[\Phi^{\text{inc}}\right] = [S]\left[\psi_{\Gamma_s}\right] + \sum_{n=1}^{m}\left[O^{1n}\right]\left[\Phi_{\Gamma_{o_n}}\right] + \sum_{n=1}^{m}\left[O^{2n}\right]\left[\psi_{\Gamma_{o_n}}\right], \tag{5}$$

where the elements of $[\Phi^{\text{inc}}]$, $[S]$, $[O^{1n}]$, and $[O^{2n}]$ are defined using the following equations:

$$\Phi_i^{\text{inc}} = \left\langle N_\Gamma^i, \Phi^{\text{inc}}\right\rangle, \tag{6}$$

$$S_{ij} = \left\langle N_\Gamma^i, -\int_{\Gamma_s} N_{\Gamma_s}^j G_0\left(\mathbf{r},\mathbf{r}'\right)d\Gamma\right\rangle, \tag{7}$$

$$O_{ij}^{1n} = \left\langle N_\Gamma^i, N_{\Gamma_{o_n}}^j - \int_{\Gamma_{o_n}}\left[N_{\Gamma_{o_n}}^j\frac{\partial G_0\left(\mathbf{r},\mathbf{r}'\right)}{\partial n}\right]d\Gamma\right\rangle, \tag{8}$$

$$O_{ij}^{2n} = \left\langle N_\Gamma^i, -\int_{\Gamma_{o_n}} N_{\Gamma_{o_n}}^j G_0\left(\mathbf{r},\mathbf{r}'\right)d\Gamma\right\rangle. \tag{9}$$

The symbol $N_\Gamma^i$ represents the basis function of the $i$th part on the boundary $\Gamma$ including $\Gamma_s$ and $\Gamma_{o_n}$. The above integral boundary equation contains $\Phi_{\Gamma_o}$, $\psi_{\Gamma_s}$, and $\psi_{\Gamma_o}$, and the number of unknowns is considerably larger than the number of equations. The above boundary integral equation cannot be solved alone, so another equation is required.

As shown in Figure 1, in every subdomain containing the object, the problem can be solved using FEM based on functional analysis theory [20]. The equivalent variational problem can be given by

$$\delta F\left(\Phi\right) = 0. \tag{10}$$

For each computed subdomain, the form of $F(\Phi)$ can be expressed as

$$\begin{aligned}F_{o_i}\left(\Phi\right) = &\frac{1}{2}\iint_{\Omega_{o_i}}\left[\frac{1}{\mu_r}\left(\frac{\partial\Phi}{\partial x}\right)^2+\frac{1}{\mu_r}\left(\frac{\partial\Phi}{\partial y}\right)^2-k_0^2\varepsilon_r\Phi^2\right]d\Omega \\ &+\int_{\Gamma_{o_i}}\Phi\psi d\Gamma \quad i=1,2,\ldots,m,\end{aligned} \tag{11}$$

where $\Omega_{o_i}$ and $\Gamma_{o_i}$ denote the $i$th interior domain and its boundary, respectively. Based on functional analysis theory, the above equations for the subdomains can be generally arranged as

$$\left[M^I\right]\left[\Phi_{o_n}^I\right] + \left[M^B\right]\left[\psi_{o_n}^B\right] = [0] \quad n=1,2,\ldots,m, \tag{12}$$

where the superscript $I$ indicates the interior space of each subdomain $\Omega_{o_n}$, and $B$ is defined as the artificial boundary $\Gamma_{o_n}$. The forms of the matrices $[M^I]$ and $[M^B]$ can be obtained from the following equation:

$$\begin{aligned}M_{ij}^I = &\iint_{\Omega_{o_n}^e}\left[\frac{\partial N_i^e}{\partial x}\frac{\partial N_j^e}{\partial x}+\frac{\partial N_i^e}{\partial y}\frac{\partial N_j^e}{\partial y}-k_0^2N_i^eN_j^e\right]dx\,dy \\ M_{ij}^B = &\int_{\Gamma_{o_n}^s} N_i^sN_j^sd\Gamma,\end{aligned} \tag{13}$$

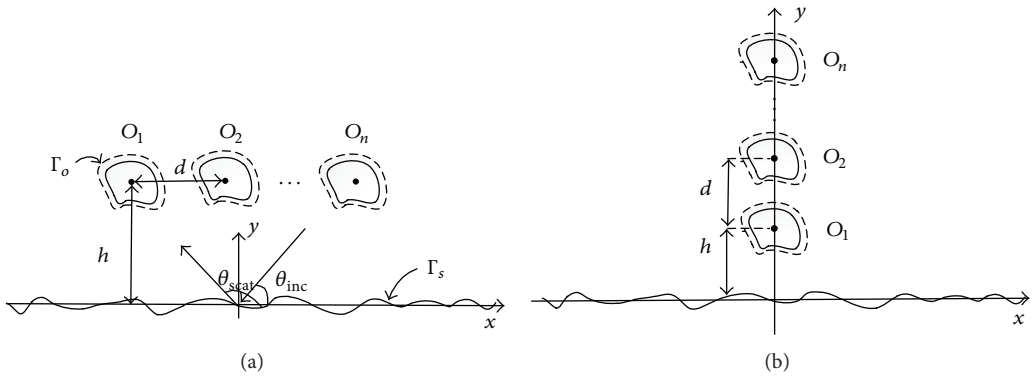


Figure 2: Schematic of the scattering from multiple dielectric objects over the PM sea surface: (a) arranged along the horizontal direction; (b) arranged along the vertical direction.

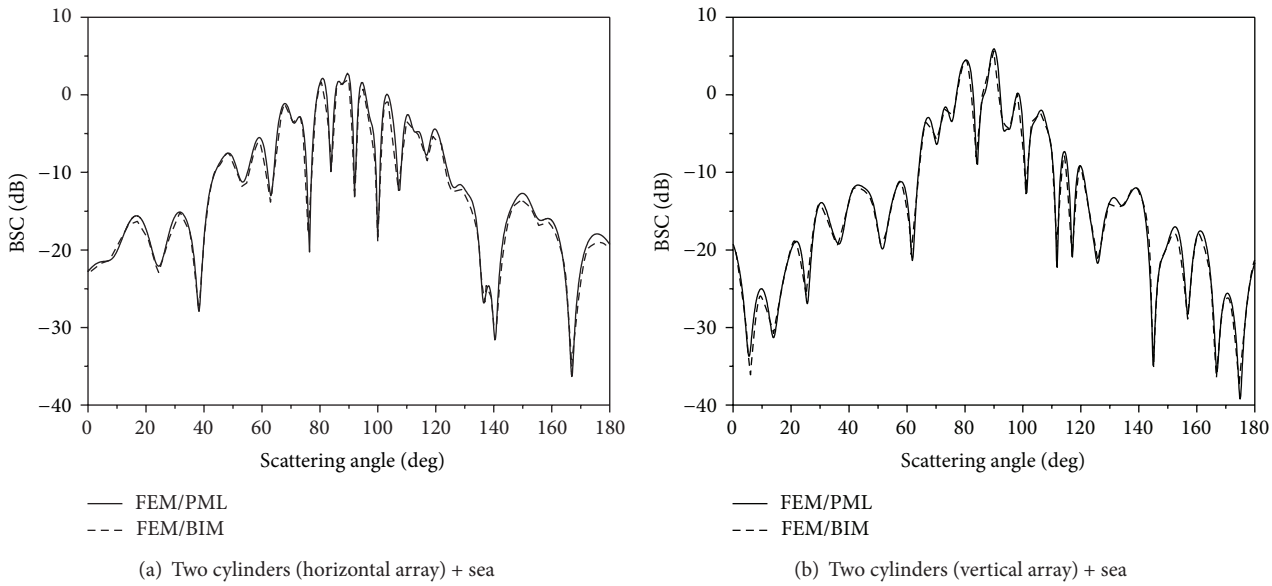


Figure 3: BSC from two cylinders over the PM rough sea surface.

where $N_i^e$ denotes the $i$th basis function of the $e$th element of the domain $\Omega_{o_n}$, and $N_i^s$ represents the $i$th basis function of the $s$th element of the boundary $\Gamma_{o_n}$

To couple (5) and (12) on the artificial boundaries $\Gamma_{o1}$, $\Gamma_{o2}$,..., $\Gamma_{o(n-1)}$, and $\Gamma_{o_n}$, the continuous conditions are applied as follows:

$$\Phi|_{\Gamma_+} = \Phi|_{\Gamma_-},$$
$$\left.\frac{\partial \Phi}{\partial n}\right|_{\Gamma_+} = \left.\frac{\partial \Phi}{\partial n}\right|_{\Gamma_-}, \tag{14}$$

where $\Gamma_+$ denotes the observation point approaching the boundaries in the exterior region, and $\Gamma_-$ expresses the observe point approaching the boundaries in the interior region. The total fields and their normal derivatives between the interior and exterior regions are contacted by (14). Using a direct linear system solver, the values of the total fields and their corresponding derivatives at every point can be calculated.

## 3. Verification of the Hybrid Method

Before FEM/BIM can be used to study the scattering properties of composite problems, the validity of our codes and the modeling technology are firstly examined in this section. In our discussion, the frequency of the incident wave is $f$ = 300 MHz, the length of the Gaussian rough surface is $L$ = 25.6 m, and the tapered factor of the incident wave is $g$ = $L/4.0$. The other parameters of the composite model, such as the incident angle $\theta_{inc}$, the altitude of the objects $h$, the relative permittivity of the object $\varepsilon_r$, the interval space between the centers of two adjacent targets $d$, the radius of the cylinders $r$ or the length of the squares $ls$, the wind speed above the sea $U_{19.5}$, and the number of the targets are all given in Figure 2.

The tapered incident wave impinges upon the model of multiple 2D objects over the 1D PM rough sea surface. As shown in Figure 2, multiple objects are arranged along the horizontal or vertical directions with a height of $h$ and symmetrically about the $y$ axis with a space of $d$ between the

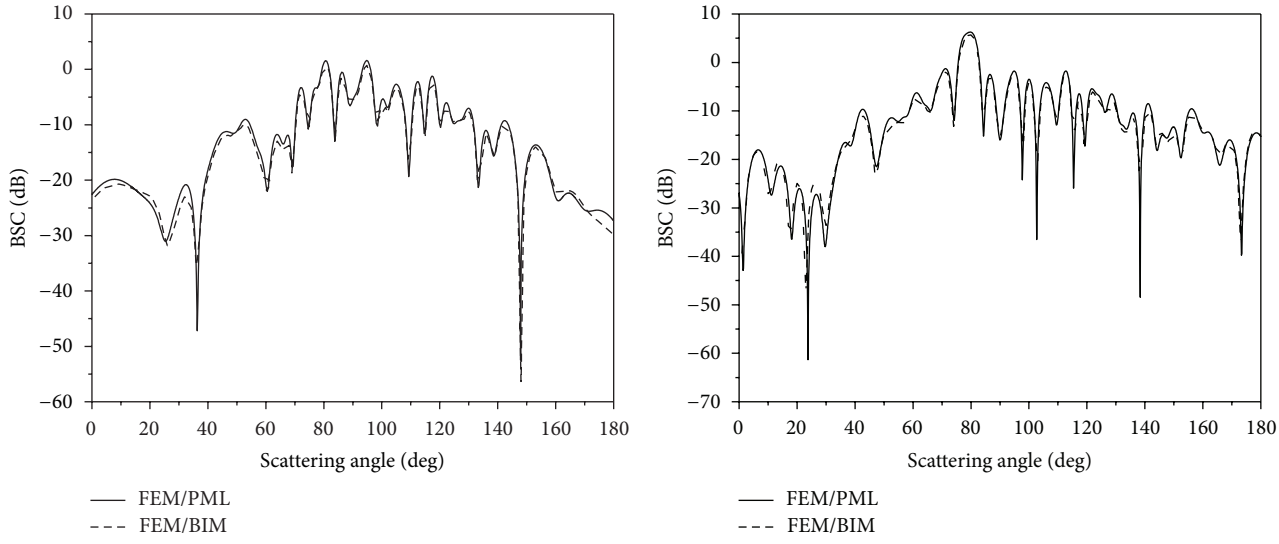


(a) Three squares(horizontal array) + sea

(b) Three squares(vertical array) + sea

Figure 4: BSC from three squares above the PM rough sea surface.

Table 1: Comparisons of solution time and number of unknowns for different methods.

| Direction of arrangement | Method | Number of unknowns | Solution time (s) |
|---|---|---|---|
| Horizontal | FEM/PML | 8316 | 14 |
| | FEM/BIM | 1028 | 0.18 |
| Vertical | FEM/PML | 13436 | 21 |
| | FEM/BIM | 1028 | 0.19 |

centers of two adjacent targets. A schematic of the scattering problem of multiple objects over the sea surface is shown in Figure 2.

To demonstrate the validity of the hybrid method, FEM/BIM is examined by the available solution of FEM/PML for one sample of the sea surface. Figure 3 gives the bistatic scattering coefficient (BSC) from two dielectric cylinders with $\varepsilon_r = 2.0 + i0.5$, ranked as in Figures 2(a) and 2(b), over the rough sea surface when the tapered wave impinges on the model. The radius of the cylinders is $r = 0.5$ m, the height of the cylinders is $h = 2.0$ m, the interval space is $d = 2.0$ m, the incident angle is $\theta_{\text{inc}} = 90^\circ$, and the wind speed is $U_{19.5} = 4$ m/s. The results of FEM/BIM agree well with FEM/PML. The reflection of the incident wave at the specular angle is very large, whereas the values of bistatic scattering in other directions are smaller than the specular angle.

Table 1 gives a comparison of solution time and number of unknowns between FEM/BIM and FEM/PML. The sparse matrix technology is used in our hybrid method, and the nonzero elements of the matrix are stored by a three-dimensional array. The sparse Gaussian elimination method is chosen as the matrix solver in this paper. The results are obtained using a computer with a 2.50 GHz processor (Intel (R) Core (TM) 2 Quad CPU), 3.47 GB memory. Table 1 shows that the number of unknowns is very large in the FEM/PML application, whereas the number of unknowns in the hybrid FEM/BIM decreases to 12.4% of those in FEM/PML for the horizontal array. In addition, the number of unknowns of objects arranged along the vertical direction is considerably larger than that in the horizontal array because the artificial boundary of PML must be set farther away from the rough surface in the vertical array than the horizontal array. However, the number of unknowns in FEM/BIM is the same in two different arrangements because the FEM region only relates to the areas of objects for hybrid FEM/BIM. For the horizontal arrangement, the solving time required for FEM/BIM is just 1.3% of those using FEM/PML. The solution time of FEM/BIM for the vertical arrangement is almost the same as that in the horizontal arrangement. However, the solution time of FEM/PML is markedly longer for the vertical array than the horizontal array.

The proposed scheme can also be confirmed using the results of FEM/PML in Figure 4, which focuses on the scattering from three dielectric squares with $\varepsilon_r = 4.0 + i1.0$ over the sea for one sample of the rough sea surface. With an interval space of $d = 2.0$ m between the centers of two adjacent squares, multiple squares are symmetrically arranged along the horizontal or vertical direction about the $y$ axis as shown in Figure 2. The length of the squares is $ls = 1.0$ m, the height of the targets is $h = 2.0$ m, and the wind above the rough sea is $U_{19.5} = 8$ m/s. The curves of our scheme highly agree with the results of FEM/PML, which indicates the feasibility of our approach for solving the composite problem of multiple targets above the rough surface. Considering that FEM/BIM is based on differential equations, increasing the mesh density or using higher order basis functions can improve the precision of the hybrid method.

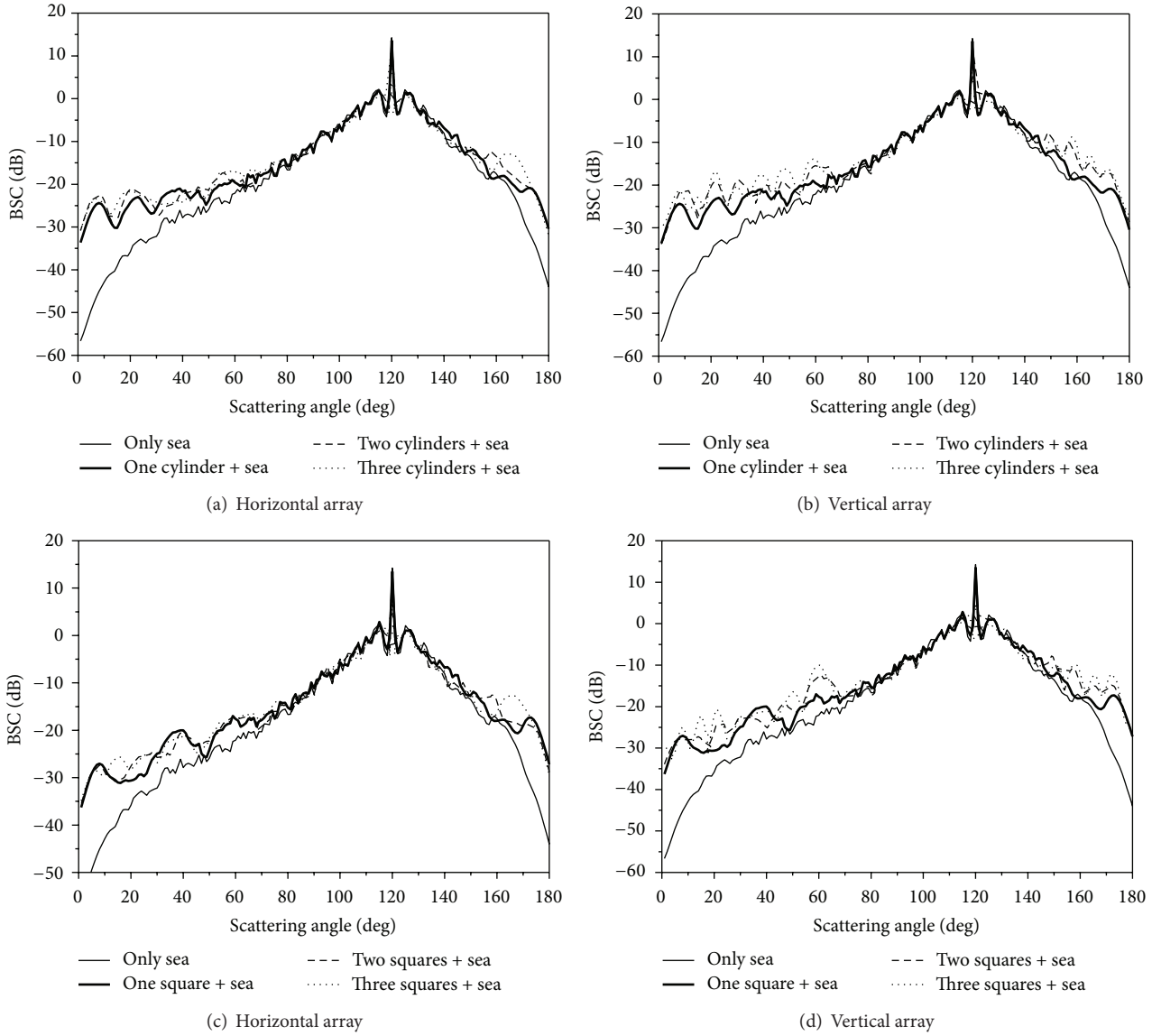


Figure 5: BSC of objects of different number over the PM rough sea surface.

Table 2: Comparisons of solution time and number of unknowns for different methods.

| Direction of arrangement | Method | Number of unknowns | Solution time (s) |
|---|---|---|---|
| Horizontal | FEM/PML | 8430 | 15 |
| | FEM/BIM | 1707 | 0.55 |
| Vertical | FEM/PML | 18670 | 26 |
| | FEM/BIM | 1707 | 0.53 |

Comparisons of the solution time and the number of unknowns between FEM/BIM and FEM/PML are shown in Table 2. The number of unknowns using FEM/BIM is 20.2% for the horizontal arrangement and 9.1% for the vertical arrangement of those in FEM/PML, respectively. The solution time required for our hybrid method is about 3.7% for the horizontal array and 2.04% for the vertical array of those in FEM/PML, respectively. The differences in the number of unknowns and the solution time between Tables 1 and 2 for FEM/BIM are mainly caused by the objects. Table 2 shows that our hybrid method is more efficient in terms of memory and time consumption than traditional FEM.

## 4. Numerical Results for Multiple Targets above Rough Sea Surface

The incident wave impinges upon the model of multiple objects above the rough sea of $L_{rs} = 102.4$ m. The radius of the cylinder is $r = 0.5$ m, and the length of the square is $ls = 1$ m. Other parameters in each of the following examples are assumed to be identical for the cylinders or squares above the sea if no special instructions are provided. The default parameters of the model are set as follows: the height of the

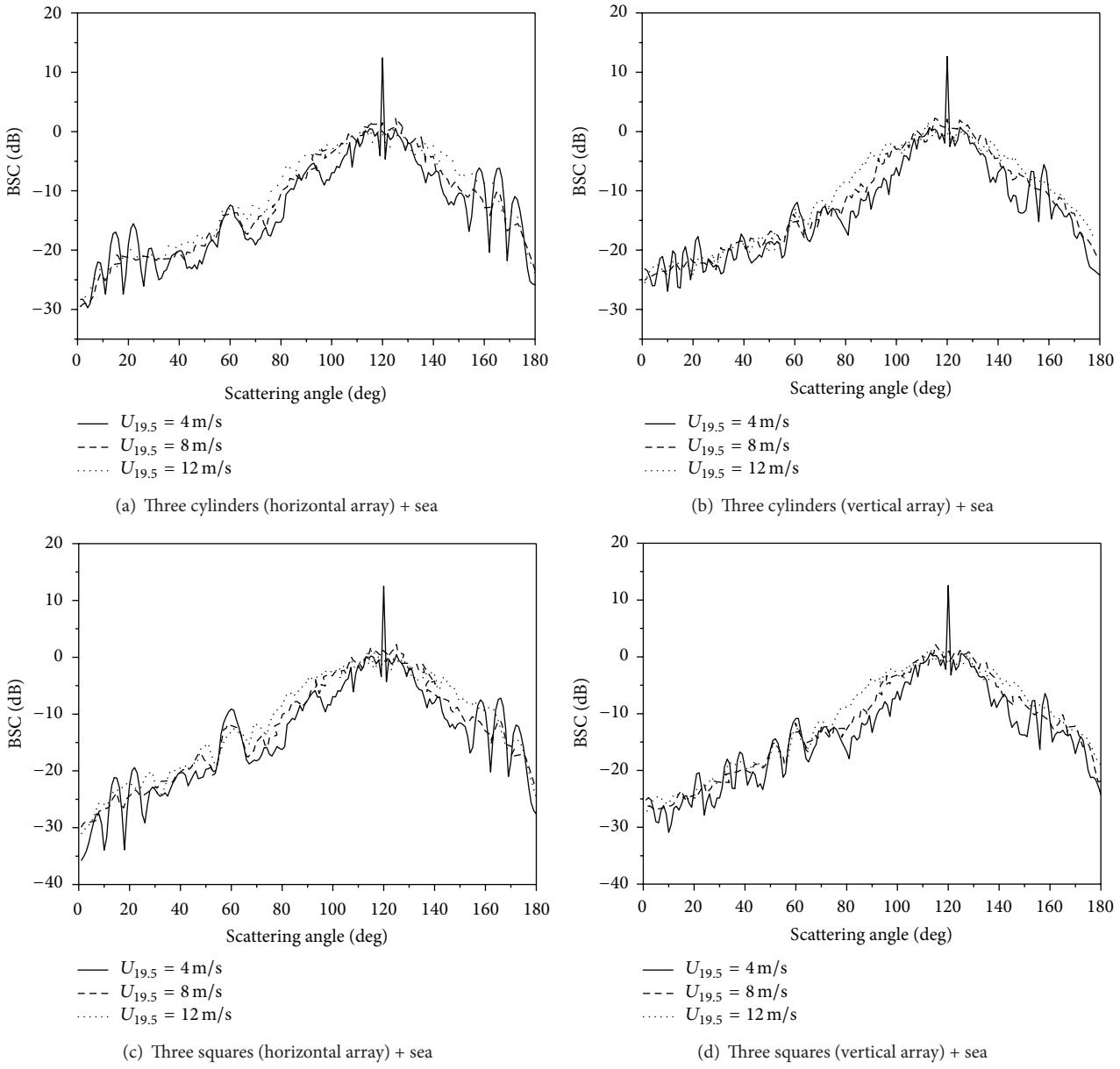


(a) Three cylinders (horizontal array) + sea

(b) Three cylinders (vertical array) + sea

(c) Three squares (horizontal array) + sea

(d) Three squares (vertical array) + sea

Figure 6: BSC of three objects over the rough sea surface of different $U_{19.5}$.

array is $h = 2$ m, the interval space of the objects is $d = 2$ m, the permittivity of the objects is $\varepsilon_r = 2 + 0.5i$, the wind speed above the sea is $U_{19.5} = 4$ m/s, and the incident angle is $\theta_{\text{inc}} = 90^\circ$. Considering the randomness of the rough surface, 30 rough surface samples are chosen, and their electromagnetic fields are averaged to obtain stable results.

To further explore the scattering characteristics of different numbers of cylinders or squares over the PM sea surface, Figure 5 shows the bistatic scattering results obtained when (1) only the rough sea surface is considered; (2) only one target exists above the sea; (3) two objects are found over the sea; and (4) three targets are found above the rough sea surface. The specular scattering from the sea is sharp and narrow, and the bistatic scattering curve is lower in the other scattering angle than those of targets existing. Figures 5(a)–5(d) show that the scattering from the composite model increases more or less when the number of objects increases, especially for the vertical array. As shown in Figures 5(a) and 5(c), when the number of objects increases, the forward scattering near 160° shows an increase brought about due to the reflection of the objects. The backward scattering near 60°increases because the vertical arrangements of the objects act as a reflective vertical wall that can reflect the incident wave back.

Figure 6 illustrates the BSC from three objects above the rough sea surface when the wind speed above the sea surface increases. In our simulation, arrays of objects are set at $h = 4$ m from the rough sea surface. The sea surface becomes

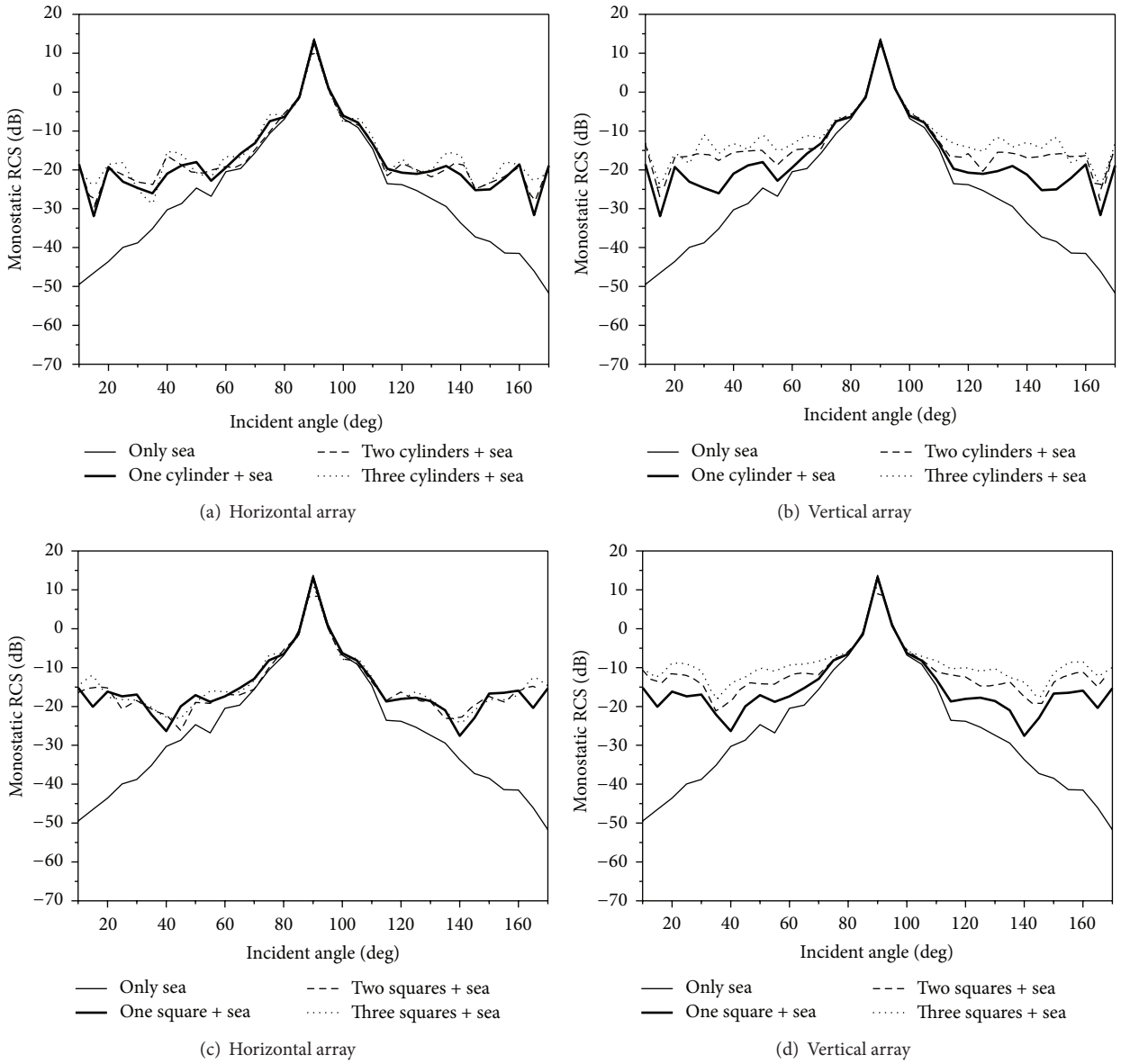


Figure 7: Monostatic RCS of objects of different number over the PM rough sea surface.

rougher when the wind speed increases, which causes an increase of the diffuse reflection. Consequently, the scattered energy is more widely distributed in nonspecular scattering directions. The curves are lower near the specular direction and higher in the scattering angle ranging from 60° to 100° and 125° to 160° with $U_{19.5}$ increasing.

Figure 7 shows the monostatic radar cross section (RCS) results when the number of the targets above the sea increases. The backscattering coefficients are similar with each other for different models when the wave impinges on the model with a vertical direction. Compared with the curves of only sea existing, the backscattering becomes stronger when the wave impinges upon the model in a large incident angle. For the horizontal array of the targets, the influence on the monostatic RCS is not very obvious when the number of the targets increases. However, the backscattering results in Figures 7(b) and 7(d) show a rise in the scattering curves with the number of the targets increasing for the vertical array.

As shown in Figure 8, the monostatic RCS results under different wind speeds are plotted. It can be seen from the results that the wind speed has an obvious influence on the backscattering when the incident angle is near 90°, and the monostatic RCS shows a decrease in the curves with the wind speed increasing. This phenomenon can be explained by the theory of diffuse reflection, and the sea becomes rougher when the wind speed increases. When the incident angle is away from 90°, the backscattering curves become strong in some incident angles for the horizontal array, and there is a decrease in some incident angles for the vertical array.

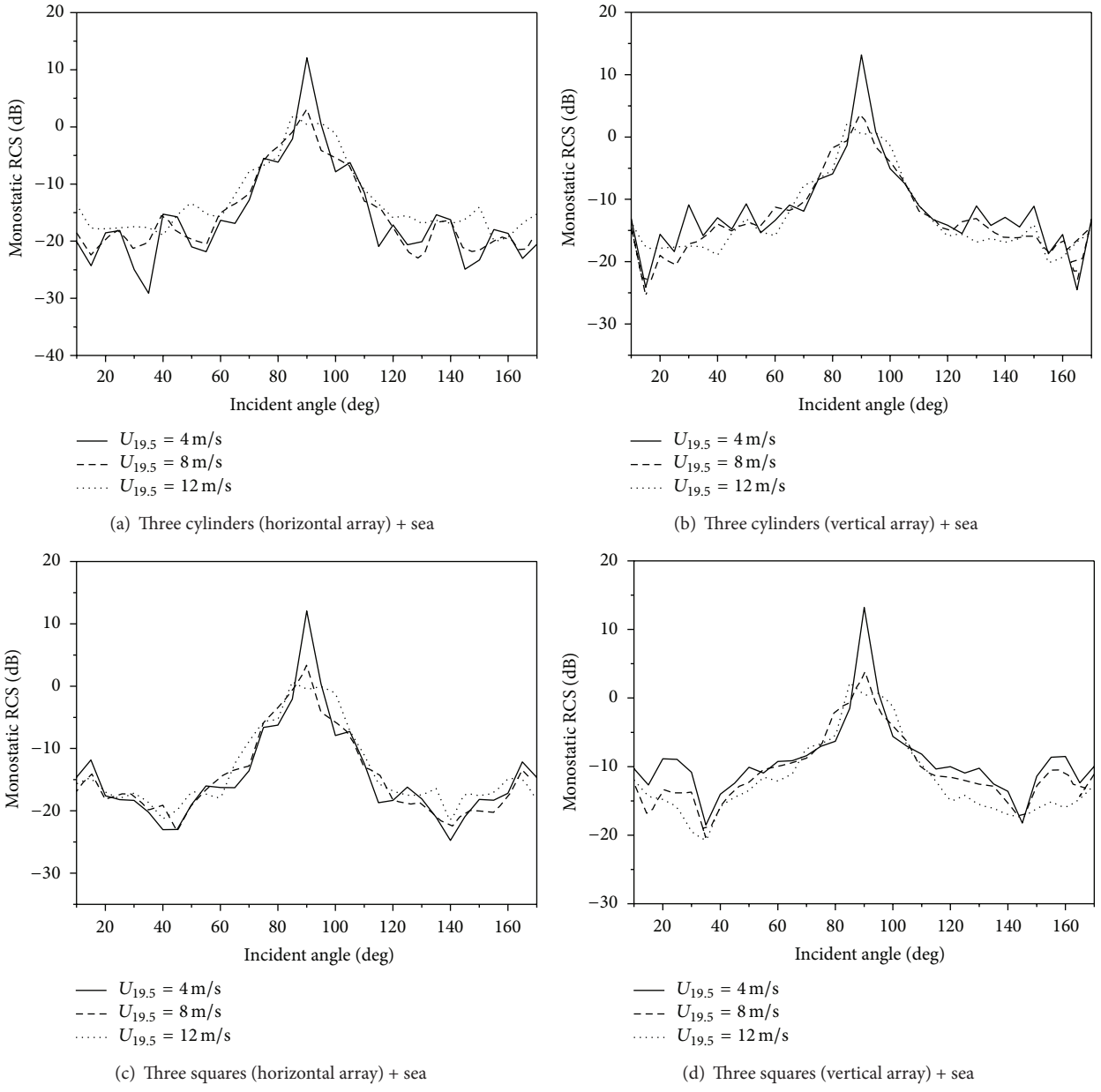


(a) Three cylinders (horizontal array) + sea

(b) Three cylinders (vertical array) + sea

(c) Three squares (horizontal array) + sea

(d) Three squares (vertical array) + sea

Figure 8: Monostatic RCS of three objects over the rough sea surface of different $U_{19.5}$.

## 5. Conclusion

In this work, an efficient strategy of hybrid FEM is proposed to investigate the scattering properties of multiple objects above the rough sea surface. In the hybrid method, FEM is only used to analyze the dielectric objects, and the rough surface is discussed using BIM. The application of the hybrid method can markedly reduce the computational region and solution time when the objects are away from the underlying rough sea surface, especially when multiple objects exist. The validity of the proposed hybrid method was verified using FEM/PML and proven to be an effective and accurate scheme. Some examples are presented to discuss the scattering from multiple objects above the rough sea surface under different conditions which can be used in signal processing applications. If this hybrid method is combined with more advanced sparse matrix technology and the node-numbering optimization, it can be expected to solve considerably large scattering problems with higher efficiency. In our future work, this topic will be investigated in detail with focus on composite scattering from three-dimensional arbitrary objects above 2D randomly rough surfaces and the accelerated techniques of hybrid FEM/BIM.

## Conflict of Interests

The authors declare that they have no financial and personal relationships with other people or organizations that can

inappropriately influence their work; there is no professional or other personal interest of any nature or kind in any product, service, and/or company that could be construed as influencing the position presented in, or the review of, the paper.

## Acknowledgments

This work was supported by the National Science Foundation for Distinguished Young Scholars of China (Grant no. 61225002), the Specialized Research Fund for the Doctoral Program of Higher Education (Grant no. 20100203110016), and the Fundamental Research Funds for the Central Universities (Grant no. K50510070001).

## References

[1] S. Y. He and G. Q. Zhu, "A hybrid MM-PO method combining UV technique for scattering from two-dimensional target above a rough," *Microwave and Optical Technology Letters*, vol. 49, no. 12, pp. 2957–2960, 2007.

[2] D. A. Kapp and G. S. Brown, "A new numerical method for rough-surface scattering calculations," *IEEE Transactions on Antennas and Propagation*, vol. 44, no. 5, pp. 711–721, 1996.

[3] M. R. Pino, F. Obelleiro, L. Landesa, and R. J. Burkholder, "Application of the fast multipole method to the generalized forward-backward iterative algorithm," *Microwave and Optical Technology Letters*, vol. 26, no. 2, pp. 78–83, 2000.

[4] O. Bakir, Ö. A. Civi, V. B. Erturk, and H. Chou, "Efficient analysis of phased arrays of microstrip patches using a hybrid generalized forward backward method/green's function technique with a DFT based acceleration algorithm," *IEEE Transactions on Antennas and Propagation*, vol. 56, no. 6, pp. 1669–1678, 2008.

[5] M. M. Botha and D. B. Davidson, "Rigorous, auxiliary variable-based implementation of a second-order ABC for the vector FEM," *IEEE Transactions on Antennas and Propagation*, vol. 54, no. 11, pp. 3499–3504, 2006.

[6] L. E. R. Petersson and J. M. Jin, "Analysis of periodic structures via a time-domain finite-element formulation with a floquet ABC," *IEEE Transactions on Antennas and Propagation*, vol. 54, no. 3, pp. 933–944, 2006.

[7] P. Liu and Y. Jin, "Numerical simulation of bistatic scattering from a target at low altitude above rough sea surface under an EM-wave incidence at low grazing angle by using the finite element method," *IEEE Transactions on Antennas and Propagation*, vol. 52, no. 5, pp. 1205–1210, 2004.

[8] O. Ozgun and M. Kuzuoglu, "Non-Maxwellian locally-conformal PML absorbers for finite element mesh truncation," *IEEE Transactions on Antennas and Propagation*, vol. 55, part 2, no. 3, pp. 931–937, 2007.

[9] Y. B. Zhai, X. W. Ping, and T. J. Cui, "Scattering from complex bodies of revolution using a high-order mixed finite element method and locally-conformal perfectly matched layer," *IEEE Transactions on Antennas and Propagation*, vol. 59, no. 5, pp. 1761–1764, 2011.

[10] O. Ozgun and M. Kuzuoglu, "Monte Carlo-based characteristic basis finite-element method (MC-CBFEM) for numerical analysis of scattering from objects on/above rough sea surfaces," *IEEE Transactions on Geoscience and Remote Sensing*, vol. 50, no. 3, pp. 769–783, 2012.

[11] M. N. Vouvakis, S. Lee, K. Zhao, and J. Lee, "A symmetric FEM-IE formulation with a single-level IE-QR algorithm for solving electromagnetic radiation and scattering problems," *IEEE Transactions on Antennas and Propagation*, vol. 52, no. 11, pp. 3060–3070, 2004.

[12] F. G. Hu and C. F. Wang, "Preconditioned formulation of FE-BI equations with domain decomposition method for calculation of electromagnetic scattering from cavities," *IEEE Transactions on Antennas and Propagation*, vol. 57, no. 8, pp. 2506–2511, 2009.

[13] Z. Peng and X. Sheng, "A flexible and efficient higher order FE-BI-MLFMA for scattering by a large body with deep cavities," *IEEE Transactions on Antennas and Propagation*, vol. 56, no. 7, pp. 2031–2042, 2008.

[14] R. Xu, L. Guo, and F. Zheng, "Application of hybrid FEM/BIE on electromagnetic scattering from random rough surface: TE case," in *Proceeding of the 10th International Symposium on Antennas, Propagation and EM Theory (ISAPE '12)*, pp. 928–931, Xian, October 2012.

[15] R. W. Xu, L. X. Guo, and T. Q. Fan, "Composite Scattering from an arbitrary dielectric target above the dielectric rough surface with FEM/PML," *Chinese Physics Letters*, vol. 30, no. 12, Article ID 124101, 2013.

[16] R. W. Xu and L. X. Guo, "An efficient hybrid method for scattering from arbitrary dielectric objects buried under a rough surface: TM case," *Optics Express*, vol. 22, no. 6, pp. 6844–6858, 2014.

[17] L. Tsang, J. A. Kong, K. H. Ding, and C. O. Ao, *Scattering of Electromagnetic Waves: Numerical Simulations*, John Wiley & Sons, New York, NY, USA, 2001.

[18] E. I. Thorsos, "The validity of the Kirchhoff approximation for rough surface scattering using a Gaussian roughness spectrum," *The Journal of Acoustical Society of America*, vol. 83, no. 1, pp. 78–92, 1988.

[19] C. A. Balanis, *Advanced Engineering Electromagnetics*, Wiley, New York, NY, USA, 1989.

[20] J. Jin, *The Finite Element Method in Electromagnetics*, Wiley, New York, NY, USA, 2002.